JCTC Journal of Chemical Theory and Computation

Homology Models and Molecular Modeling of Human Retinoic Acid Metabolizing Enzymes Cytochrome P450 26A1 (CYP26A1) and P450 26B1 (CYP26B1)

Magnus Karlsson,[†,‡] Åke Strid,[†] Allan Sirsjö,[§] and Leif A. Eriksson*[,†]

Department of Natural Sciences and Örebro Life Science Center, Modeling and Simulation Research Center, and Department of Clinical Medicine, Örebro University, 70182 Örebro, Sweden

Received January 30, 2008

Abstract: Homology models of cytochrome P450 26A1 and cytochrome P450 26B1 were constructed using the crystal structures of human, CYP2C8, CYP2C9, and CYP3A4 as templates for the model building. The homology models generated were investigated for their docking capacities against the natural substrate all-*trans*-retinoic acid (atRA), five different tetralone-derived retinoic acid metabolizing blocking agents (RAMBAs), and R115866. Interaction energies (IE) and linear interaction energies (LIE) were calculated for all inhibitors in both homology models after molecular dynamics (MD) simulation of the enzyme−ligand complexes. The results revealed that the homologues had the capacity to distinguish between strong and weak inhibitors. Important residues in the active site were identified from the CYP26A1/B1−atRA complexes. Residues involved in hydrophobic interactions with atRA were Pro113, Phe222, Phe299, Val370, Pro371, and Phe374 in CYP26A1 and Leu88, Pro118, Phe222, Phe295, Ile368, and Tyr272 in CYP26B1. Hydrogen bonding interactions were observed between the atRA carboxylate group and Arg 90 in CYP26A1 and with Arg76, Arg95, and Ser369 in CYP26B1.

1. Introduction

Retinoic acid (RA) is the most active metabolite of vitamin A and is present in a multitude of human tissues.[1] It plays a crucial role in growth and differentiation during embryogenesis and organogenesis but also in regulation of gene expression, cellular differentiation and proliferation of epithelial cells. The all-*trans*-retinoic acid isomer (atRA) has been studied in a number of clinical situations, especially in oncology against promyelocytic leukemia[2] and in dermatology against cystic acne and photodamaged skin.[3] However, because there are common mechanisms underlying cancer and cardiovascular diseases, the use of retinoids may also show therapeutic value in some cardiovascular diseases. Restenosis and arteriosclerosis are initiated by endothelial injury in the vessel. During injury, the regulation of vascular homeostasis is disturbed leading to induction of smooth muscle cell (SMC) dedifferentiation, growth and migration.[4,5] The processes in a vessel following balloon angioplasty have been studied in animal models.[4] These studies show that atRA has the ability to reduce neointimal growth and increase the luminal area. The fact that retinoids are involved in the regulation of a variety of cellular processes suggests that they have potential abilities as therapeutic agent against vascular disorders.[6]

A rapid decrease in plasma levels of atRA has been observed in acute promyelocytic leukemia patients, which indicates an autoregulatory mechanism and the ability of atRA to induce its own catabolism.[7] This main pathway of atRA metabolism starts with hydoxylation at the C-4 position of the cyclohexenyl ring.[8] Although many microsomal cytochrome P450 enzymes are capable to initiate atRA metabolism through 4-hydroxylation, their specificity is generally low.[9] CYP26, a new family of cytochrome P450

* Corresponding author e-mail: leif.eriksson@nat.oru.se.

[†] Department of Natural Sciences and Örebro Life Science Center, Örebro University.

[‡] Modeling and Simulation Research Center, Örebro University.

[§] Department of Clinical Medicine and Örebro Life Science Center, Örebro University.

10.1021/ct800033x CCC: $40.75
Published on Web 05/02/2008

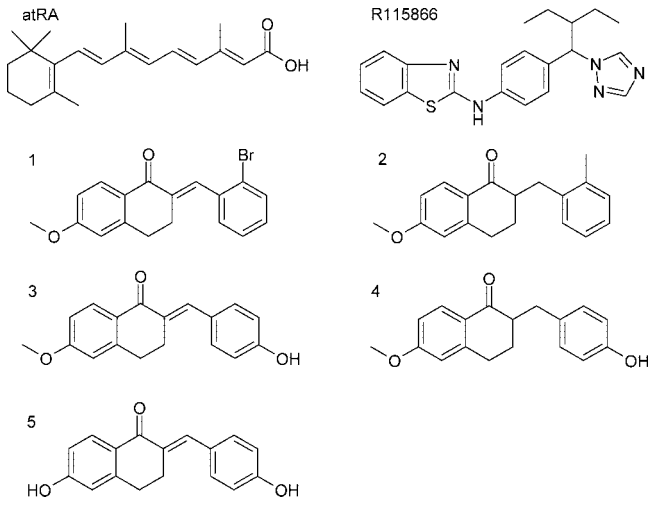

Figure 1. Ligands used for evaluation of docking capabilities in the CYP26A1 and CYP26B1 homology models. 1−5: tetralone-derived RAMBAs reported by Yee et al.[22]

enzymes, consists of three members, CYP26 A1, B1, and C1, that metabolize atRA mainly into 4-OH-RA but also to 5,6-epoxy-RA and 18-OH-RA. CYP26A1 and B1 have high specificity for atRA, whereas CYP26C1 efficiently metabolizes both atRA and 9-*cis*-RA.[10,11] CYP26B1 seems to be upregulated by lower concentrations of atRA than CYP26A1 in intimal SMCs which suggests that CYP26B1 is the dominating isoform in this celltype.[12] The discovery of retinoic acid response elements on the CYP26 promoter by Loudig et al. revealed the mechanism by which atRA induces the mRNA expressions of CYP26s.[13]

Fast metabolism and CYP26-mediated resistance are the main causes behind the search for inhibitors against CYP-mediated metabolism of atRA. The antimycotic substance ketoconazole was the first compound evaluated as a potential inhibitor against atRA metabolizing enzymes. Van Wauwe et al. demonstrated in their studies that ketoconazole prolonged the half-life of exogenously administrated atRA to animals.[14] Unfortunately, adverse side effects were observed for ketoconazole. Extensive structure−activity relationship studies on imidazole derivatives resulted in the discovery of liarozole, which is the most studied retinoic acid metabolism blocking agent (RAMBA) so far. The antitumoral effects of liarozol shown in animal studies correlate with an increase in tumor differentiation, following accumulation of atRA.[15] Liarozole has been a lead compound in the search for other RAMBAs. New inhibitors with high potency and specificity for atRA-cytochrome P450 hydroxylase based on liarzole as standard have been designed and evaluated.[16] Triazole derivatives R115866 and R116010 are highly potent (100-fold more potent than liarozole itself) and selective second-generation inhibitors of CYP26-induced atRA metabolism. R116010 was demonstrated to inhibit RA-metabolism, subsequently leading to inhibition of tumor growth at lower concentrations than atRA.[17] Stoppie et al. demonstrated the inhibitory effects of R115866 on atRA metabolism in rodents, which resulted in increased endogenous atRA and retinoidal effects including inhibition of vaginal hyperkeratinization.[18] Besides of R115866 and R116010, a large number of new RAMBAs have been reported with prominent inhibitory ability against CYP26. Recent studies of azolyl retenoids,[19] benzenacetic acid derivates[20] and 2,6-distributed naphtalenes[21] have resulted in new candidates for therapeutic use.

Lack of crystal structures of CYP26A1 and CYP26B1 makes virtual screening in the search for new and improved inhibitors difficult. In this study, bioinformatics and molecular mechanics tools necessary to generate new homologies of CYP26A1 and B1 have been utilized. The architectures of the active site of the homology models have been investigated and evaluated by their docking capabilities against known CYP26A1 inhibitors recently reported in the literature,[22] Figure 1. The homology model of CYP26A1 is also compared with the only previous homology model of CYP26A1 available, reported by Gomaa et al.[23] For CYP26B1, the current study represents the first model of that enzyme.

2. Materials and Methods

Computational Approaches. All molecular modeling was performed using the Molecular Operating Environment (MOE) 2005.06 and 2006.08 programs.[24,25] All structures of ligands, CYP26A1 and CYP26B1 models, and water−ligand and enzyme−ligand complexes were geometry minimized using the AMBER99 molecular mechanics force field[26] to within an rms gradient of 0.5 kcal mol^{-1} $Å^{-1}$. All water−ligand complexes were formed by adding a sphere of water molecules containing a layer width of 10 Å. Throughout, all systems were also surrounded by a distance dependent dielectric model.[27]

To obtain relaxed geometries, short molecular dynamics (MD) simulations were performed, followed by a final energy minimization step. The MD simulations on the CYP26A1 and CYP26B1 models, water−ligand, and enzyme−ligand complexes were performed using a canonical ensemble, NVT, with initial temperature 150 °K; heating for 50 ps; simulation temperature 300 °K; duration 500 ps; time step 1 fs (2 fs for water-ligand-complexes); temperature response 1 ps; pressure response 0.5 ps and constraint tolerance 1×10^{-9} ps. The haem group and the Fe−N or Fe−O distances to inhibitors with triazole or alcohol groups were held fixed during the simulations.

Model Building. The protein sequences of human CYP26A1 and CYP26B1 were obtained from the NCBI server (no. 2688846 and no. 9845285). Homology models of CYP26A1 and CYP26B1 were built using crystal structures of human CYP2C8 (PDB no. 1PQ2), CYP2C9 (PDB no. 1OG2) and CYP3A4 (PDB no. 1TQN) as templates.[23] Sequence similarity between CYP26A1 and B1, and the three template structures, was between 22 and 24% for all systems. Sequence alignment was performed in the MOE-align panel using default settings with alignment constraints on the haem cysteine residue, the query sequence, and the corresponding templates. CYP3A4 was used as primary template (Figure 2) and the homology models were built taking the best of ten intermediate models minimized to within a rms gradient of 0.1. The haem group was inserted and positioned with the same coordinates as the primary template, and protonation state of titratable groups at pH 7.4 were calculated.

```
CYP26A1     -----MGLPALLASALCTFVLPLLLFLAAIKLWDLYCVSGRDRSCALPLP 45
CYP26B1     MLFEGLDLVSALATLAACLVSVTLLLAVSQQLWQLRWAATRDKSCKLPIP 50
CYP3A4      ------------MDLIPNFAMETWVLVATSLVLLYIYGTHSHKLFKKLGI 38
                              :.    :: .:  :      :  .:

CYP26A1     PGTMGFPFFGETLQMVLQRRKFLQMKRRKYGFIYKTHLFGRPTVRVMGAD 95
CYP26B1     KGSMGFPLIGETGHWLLQGSGFQSSRREKYGNVFKTHLLGRPLIRVTGAE 100
CYP3A4      PGPTPLPFLGTILFYLRGLWNFDRECNEKYGEMWGLYEGQQPMLVIMDPD 88
             *.  :*::*     :     *    ..*** ::  :   :* : : ..:

CYP26A1     NVRRILLGEHRLVSVHWPASVRTILGSGCLSNLHDSSHKQRKKVIMRAFS 145
CYP26B1     NVRKILMGEHHLVSTEWPRSTRMLLGPNTVSNSIGDIHRNKRKVFSKIFS 150
CYP3A4      MIKTVLVKECYSVFTNQMPLGPMGFLKSALSFAEDEEWKRIRTLLSPAFT 138
             :: :*: *   * ..        :  . :*   ..  :. :.::   *:

CYP26A1     REALECYVPVITEEVGSSLEQWLSCGERGLLVYPEVKRLMFRIAMRILLG 195
CYP26A1     HEALESYLPKIQLVIQDTLRAWSSHP-EAINVYQEAQKLTFRMAIRVLLG 200
CYP3A4      SVKFKEMVPIISQCGDMLVRSLRQEAENSKSINLKDFFGAYTMDVITGTL 188
               ::  :* *       :.   .   ..  :  :     : : :

CYP26A1     CEPQLAGDGDSEQQLVEAFEEMTRNLFSLPIDVPFSGLYRGMKARNLIHA 245
CYP26B1     FSIPEEDLG----HLFEVYQQFVDNVFSLPVDLPFSGYRRGIQARQILQK 246
CYP3A4      FGVNLDSLNNPQDPFLKNMKKLLKLDFLDPFLLLISLFPFLTPVFEALNI 238
                  . .     :.:  :::    *  *. : :*       . : ::

CYP26A1     R--------IEQNIRAKICGLRASEAGQGCKDALQLLIEH----SWERGE 283
CYP26A1     G--------LEKAIREKLQ----CTQGKDYLDALDLLIES----SKEHGK 280
CYP3A4      GLFPKDVTHFLKNSIERMKESRLKDKQKHRVDFFQQMIDSQNSKETKSHK 288
                      : :    ::         :   * :: :*:     . :  :

CYP26A1     RLDMQALKQSSTELLFGGHETTASAATSLITYLGLYPHVLQKVREELKSK 333
CYP26B1     EMTMQELKDGTLELIFAAYATTASASTSLIMQLLKHPTVLEKLRDELRAH 330
CYP3A4      ALSDLELVAQSIIIIFAAYDTTSTTLPFIMYELATHPDVQQKLQEEIDAV 338
             :    *   :  ::*..: **::: . ::  *  :* * :*:::*: :

CYP26A1     GLLCKS--NQDNKLDMEILEQLKYIGCVIKETLRLNPPVPGGFRVALKTF 381
CYP26B1     GILHSGGCPCEGTLRLDTLSGLRYLDCVIKEVMRLFTPISGGYRTVLQTF 380
CYP3A4      LPNKAP-------VTYDALVQMEYLDMVVNETLRLFPVVSRVTRVCKKDI 381
                         :  : *  :.*:. *::*.:** . :.   *.  : :

CYP26A1     ELNGYQIPKGWNVIYSICDTHDVAEIFTNKEEFNPDRFMLPHPEDAS-RF 430
CYP26B1     ELDGFQIPKGWSVMYSIRDTHDTAPVFKDVNVFDPDRFSQARSEDKDGRF 430
CYP3A4      EINGVFIPKGLAVMVPIYALHHDPKYWTEPEKFCPERFSKKN-KDSIDLY 430
            *::*  ****  *: .*   *. .  :.: : * *:**   . :*    :

CYP26A1     SFIPFGGGLRSCVGKEFAKILLKIFTVELAR--HCDWQLLN-GPPTMKTS 477
CYP26B1     HYLPFGGGVRTCLGKHLAKLFLKVLAVELAS--TSRFELATRTFPRITLV 478
CYP3A4      RYIPFGAGPRNCIGMRFALTNIKLAVIRALQNFSFKPCKETQIPLKLDNL 480
             ::***.* *.*:* .:*   :*: .:.            .     :

CYP26A1     PTVYPVDNLPARFTHFHGEI---------------497
CYP26B1     PVLHPVDGLSVKFFGLDSNQNEILPETEAMLSATV 512
CYP3A4      PILQPEKPIVLKVHLRDGITSGP------------503
            * : * . :  :.   ..
```

Figure 2. Sequence alignment of CYP26A1, CYP26B1, and CYP3A4 with ClustalW (1.81). "*", identical residues; ":", conserved constitution; and ".", semiconserved.

Docking. Possible active sites in the receptor homology models were identified by using Alpha Site Finder.[28] Once defined, ligands were docked into the enzyme with a retain of 500 poses using the alpha triangle placement methodology with affinity ΔG as scoring function.[25] In the docking studies, flexible ligand structures were generated suing a Monte Carlo algorithm, whereas the receptors were held fixed according to the minimized geometries.

Energy Calculations of the Enzyme−Ligand Complex. The potential energies of the whole system after MD-simulation and minimization for the enzyme-ligand-complex (EL) as well as for the unbound ligand and enzyme (E+L) were calculated. The interaction energy (IE) was obtained by taking the energy difference between the two systems.

$$I_E = E_{TOT}(EL) - E_{TOT}(E+L) \quad \text{(kcal/mol)} \qquad (1)$$

The binding free energies of the ligands were calculated through the linear interaction energy (LIE). LIE basically depicts the ligand as being solvated in two different media: water and the macromolecule.[29]

$$\Delta G = \alpha\Delta(U_{e-w}^{vdw}) + \beta\Delta(U_{e-w}^{el}) \quad \text{(kcal/mol)} \qquad (2)$$

In eq 2, the ensemble averages of the interaction energies, $\Delta(U_{e-w}^{vdw})$ and $\Delta(U_{e-w}^{el})$ were obtained by calculating the van

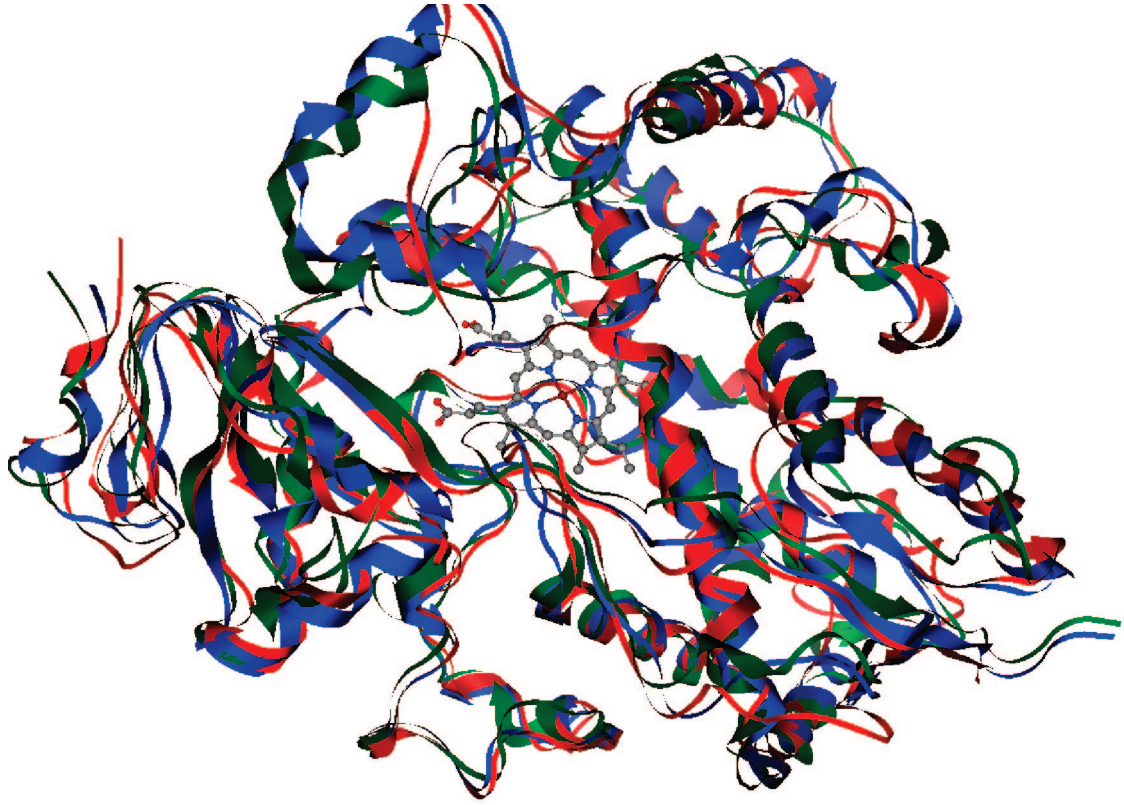

Figure 3. Superposed backbones of homologes; CYP26A1 in red, CYP26B1 in green, and CYP3A4 (1TQN-A) in blue.

der Waals and electrostatic interaction energies from ten MD trajectories for ligands free in water (w) and ligand bound to the enzyme (e). α was set to 0.9 for all compounds and β was set to 0.37 for alcohols and 0.43 for all other compounds.

3. Results and Discussion

The homology models of CYP26A1 and B1 superpose well with each other and with the major template CYP3A4, Figure 2 and 3. From the RAMPAGE server,[30] the percentage of conformations in favored regions obtained from Ramachandran plots of the superposed structures in Figure 3 was calculated to 82.9%. The active sites however display some interesting differences in architecture between the created homologes. In the CYP26 models, atRA was docked into active site orientated for oxidation with the C4 atom positioned 4.71 Å from the haem iron in CYP26A1 and 5.08 Å in CYP26B1, Figure 4. AtRA formed multiple hydrophobic interactions with the amino acid residues Pro113, Phe222, Phe299, Val370, Pro371, and Phe374 in CYP26A1 and with Leu88, Pro118, Phe222, Phe295, Ile368, and Tyr272 in CYP26B1.

Of these, equivalent residues located in the active site between the A1−B1 models were Pro113-Pro118, Phe222-Phe222, and Phe299-Phe295. Even if there are similarities, the architecture between these two homology models has sufficient differences in their active sites to render possibilities to create a selective inhibitor for each of them. In particular, the significantly large number of hydrogen bonding groups in the active site of B1 could serve as an important discriminatory factor.

Evaluation of the homology models of CYP26A1 and B1 was performed by docking known inhibitors reported in literature and calculating the properties, Figure 1. All experimental data was obtained from a MCF-7 (CYP26A1) assay for metabolic inhibition of atRA reported by Yee et al.[22]. No experimental data for inhibition of atRA metabolism in CYP26B1 is available for the inhibitors studied in this paper. The results from the CYP26B1 calculations are thus comparable only to experimental and theoretical data from CYP26A1. It should be emphasized that, as atRA is a charged acid, whereas the now studied inhibitors are not, comparison of interaction energies between inhibitors and atRA become less valid.

The theoretically calculated values for the tetralone-derived RAMBAs and R115866 in CYP26A1 agree well with the trends seen in the experimental IC_{50} data reported by Yee et al.; Table 1. Tetralone 5 was the only inhibitor that stabilized the complex (-43.44 kcal/mol) more than it should according to the experimental findings. Interestingly, tetralone 5 also represented a slightly lower free energy value (−2.63 kcal/mol) from the LIE calculation compared to the other tetralones, Table 1. One possible explanation for this behavior could be that tetralone 5 has two hydroxyl-groups in its structure, which results in increased interaction between the ligand and the enzyme when comparing with the free ligand, whereas in the LIE calculations, the "free ligand" is surrounded by hydrogen bonding water molecules. This gives an enhanced IE in the enzyme−ligand complex, but a reduced binding free energy (ΔG) from the LIE analysis.

As seen from the computed data in Tables 1 and 2, the homology models developed in this work were capable of

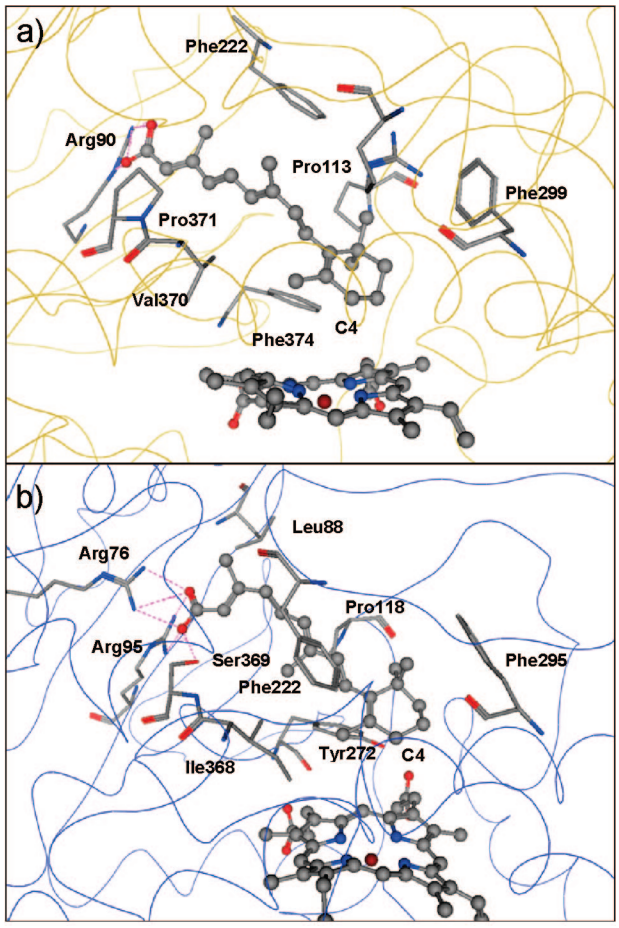

Figure 4. Active site after MD simulation of (a) CYP26A1 and (b) CYP26B1 with atRA bound. Key amino acids in stick-drawing, atRA, and haem group in ball-and-stick. Hydrogen bonds displayed as pink lines.

differentiating between "weak inhibitors" and the potent inhibitor R115866 in both CYP26A1 and CYP26B1. However, the theoretically calculated values differ between the homology models of CYP26A1 and CYP26B1. The interaction energies for the tetralones in CYP26B1, Table 2, are generally lower compared to CYP26A1, Table 1. The calculated values for the tetralones containing hydroxy-groups (tetralones 3, 4, and 5) in the CYP26B1 model differed most compared to the experimental and calculated data for CYP26A1. In Figure 5 we display the calculated interaction energies vs IC_{50} values (5a), and the calculated free energy of interaction based on LIE analysis (5b), respectively. The different LIE data for tetralone 3−5 indicate the possibility to find a selective inhibitor specific toward either A1 or B1.

Further, the tetralones in the active site seems to reach inhibitory effects in different ways. Tetralones 1 and 2 could not form any explicit interactions with the haem iron because of the lack of hydroxyl groups in their structures. Instead, they obtained their inhibitory effect mainly through hydrophobic interactions by acting in an atRA mimetic way. Tetralones 3 − 5 binds to the haem iron through their 4-hydroxyphenyl substituent, resulting in additional inhibitory activity in most cases. Tetralone 5, with an additional hydroxyl substituent, manages to obtain hydrogen bonding with Arg 90 in the CYP26A1 model and with Arg 95 in the CYP26B1 model. One essential residue for hydrophobic interactions between the tetralones and the active sites in both models is Phe222.

Comparing the CYP26A1 homologue reported by Gomaa et al. with the CYP26A1 homology model created in this study displays some differences in the active site architecture and position of atRA. In this study, the distance between the C4 atom on the cyclohexyl ring in atRA and the haem iron was 4.71Å, which is closer than the distance reported by Gomaa et al. (5.3Å). The residues in the active site involved in hydrophobic interaction are almost identical. Residues Phe222, Phe299, Pro371, and Phe374 are synonymous in both studies while Pro113 and Val370 in the current model replaced Trp112 and Phe84. The biggest difference

Table 1. Interaction Energy (eq *1*) and Linear Interaction Energy (eq *2*) Calculations from MD-Simulated CYP26A1 Complexes (kcal/mol)

ligand	IC50 (μM)[a]	E_{TOT}	E_M	I_E	$\alpha\Delta(U_{e-w}^{vdw})$	$\beta\Delta(U_{e-w}^{el})$	ΔG
atRA	inducer						
R115866	0.005	−6945.28	−6891.03	−54.25	5.943	−18.874	−12.93
tetralon 1	9	−7016.87	−6975.56	−41.31	10.451	−13.451	−3.00
tetralon 2	30	−7077.84	−7043.90	−33.94	5.046	−5.793	−0.75
tetralon 3	7	−6948.66	−6905.82	−42.86	9.600	−13.700	−3.10
tetralon 4	5	−6876.57	−6830.80	−45.57	5.646	−11.906	−6.26
tetralon 5	9	−6986.61	−6943.17	−43.44	9.418	−12.047	−2.63

[a] Results obtained from MCF-7 CYP26A1 cell assay reported by Yee et al.[22]

Table 2. Interaction Energy (eq *1*) and Linear Interaction Energy (eq *2*) Calculations from MD-Simulated CYP26B1 complexes (kcal/mol)

ligand	IC50 (μM)[a]	E_{TOT}	E_M	I_E	$\alpha\Delta(U_{e-w}^{vdw})$	$\beta\Delta(U_{e-w}^{el})$	ΔG
atRA	inducer						
R115866	0.005	−6464.79	−6410.79	−54.00	5.233	−16.609	−11.38
tetralon 1	9	−6563.46	−6520.57	−42.89	10.176	−13.861	−3.69
tetralon 2	30	−6564.84	−6528.83	−36.01	4.494	−5.054	−0.56
tetralon 3	7	−6618.86	−6572.32	−46.54	8.408	−15.224	−6.82
tetralon 4	5	−6508.45	−6461.30	−47.15	2.767	−6.800	−3.35
tetralon 5	9	−6611.97	−6571.48	−40.49	10.744	−15.458	−4.71

[a] Results obtained from MCF-7 CYP26A1 cell assay reported by Yee et al.[22]

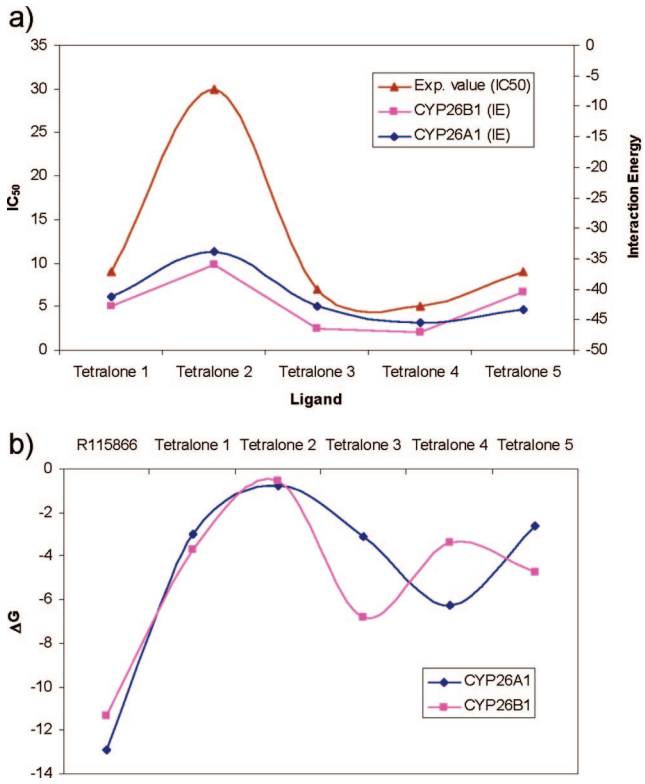

Figure 5. Comparison of (a) interaction energies of tetralone derived RAMBAs in CYP26A1 and B1 with experimental data in MCF-7 CYP26A1 cell assay[22] and (b) linear interaction energies of R115866 and tetralone derived RAMBAs in CYP26A1 and B1.

between the two models is however the residue hydrogen bonding to the carboxyl group in atRA. In our model, it binds to Arg90, whereas in the model by Gomaa et al. it binds to Arg86. We furthermore note that although the Ramachandran plots for our superposed structure in Figure 3 gave 82.9% of the conformations in favored regions, Gomaa et al.[23] obtained 81.4% for their CYP26A1-CYP3A4 model.

The differences in the active site can be explained by how the homologues were built, and which forcefield and algorithm that was used. Gomaa et al. used MOE 2004.03 with the CHARMM22 molecular mechanics forcefield and the Cartesian average model to generate the homologue. Ligands were docked using the FlexX docking of SYBYL, and the MD simulations were performed with Gromacs 3.2 in the Gromacs forcefield with a time step of 2 fs during 800 ps.

Conclusions

We have in the current work created homology models of the retinoic acid-metabolizing cytochromes, CYP26A1 and CYP26B1, and evaluated the models by docking, MD-simulation and calculation of the IE and LIE of known inhibitors bound in the active site. The IE calculations are in very good agreement with experimental data, Table 1 and 2, showing that the created models are reliable and suitable for use of further analysis in finding new RAMBAs. The results also illustrate the homologues ability to distinguish between novel and highly potent RAMBAs. The study also indicates different interactions with the active site for the inhibitors. Tetralones 1 and 2 obtained their inhibitory effects mainly through hydrophobic interactions but do not form any explicit interaction with the haem iron. Tetralones 3−5 and R115866; on the other hand, bind to the haem iron through their hydroxyl or triazole groups resulting in additional inhibitory activity in most cases. The differences in residue composition between the active sites in CYP26A1 and CYP26B1 and LIE data for tetralones 3−5 indicate the possibility of finding a selective inhibitor specific toward either A1 or B1.

Acknowledgment. We acknowledge the Modeling and Simulation Research Center (MoS) at Örebro University for a PhD scholarship grant (M.K.), and the support from the faculties of Science and Technology (L.A.E., Å.S.) and Medicine (A.S.) for additional funding. The work was also supported by the Swedish Science Research Council (VR).

References

(1) Russell, R. M.; Ross, A. C.; Trumbo, P. R.; West, K. P. Retinol equivalency ratio of beta-carotene. *J. Nutr.* **2003**, *133*, 2915–2916.

(2) Estey, E. H.; Giles, F. J.; Kantarjian, H.; O'Brien, S.; Cortes, J.; Freireich, E. J.; Lopez-Berestein, G.; Keating, M. Molecular remissions induced by liposomal-encapsulated all-trans retinoic acid in newly diagnosed acute promyelocytic leukemia. *Blood* **1999**, *94*, 2230–2235.

(3) Ahmad, N.; Mukhtar, H. Cytochrome P450: A target for drug development for skin diseases. *J. Invest. Dermatol.* **2004**, *123*, 417–425.

(4) Miano, J. M.; Kelly, L. A.; Artacho, C. A.; Nuckolls, T. A.; Piantedosi, R.; Blaner, W. S. all-trans-retinoic acid reduces neointimal formation and promotes favorable geometric remodeling of the rat carotid artery after balloon withdrawal injury. *Circulation* **1998**, *98*, 1219–1227.

(5) Gidlof, A. C.; Ocaya, P.; Krivospitskaya, O.; Sirsjo, A. Vitamin A: a drug for prevention of restenosis/reocclusion after percutaneous coronary intervention. *Clin. Sci.* **2008**, *114*, 19–25.

(6) Gidlof, A. C.; Romert, A.; Olsson, A.; Torma, H.; Eriksson, U.; Sirsjo, A. Increased retinoid signaling in vascular smooth muscle cells by proinflammatory cytokines. *Biochem. Biophys. Res. Commun.* **2001**, *286*, 336–342.

(7) Muindi, J.; Frankel, S. R.; Miller, W. H.; Jakubowski, A.; Scheinberg, D. A.; Young, C. W.; Dmitrovsky, E.; Warrell, R. P. Continuous Treatment with All-Trans Retinoic Acid Causes a Progressive Reduction in Plasma Drug Concentrations - Implications for Relapse and Retinoid Resistance in Patients with Acute Promyelocytic Leukemia. *Blood* **1992**, *79*, 299–303.

(8) Napoli, J. L. Retinoic acid biosynthesis and metabolism. *Faseb J.* **1996**, *10*, 993–1001.

(9) McSorley, L. C.; Daly, A. K. Identification of human cytochrome P450 isoforms that contribute to all-trans-Retinoic Acid 4-hydroxylation. *Biochem. Pharmacol.* **2000**, *60*, 517–526.

(10) White, J. A.; Becket Jones, B.; Guo, Y. D.; Dilworth, F. J.; Bonasoro, J.; Jones, G.; Petkovich, M. cDNA cloning of human retinoic acid-metabolizing enzyme (hP450RAI) identifies a novel family of cytochromes P450 (CYP26). *J. Biol.*

Chem. **1997**, *272*, 18538–18541.

(11) Taimi, M.; Helvig, C.; Wisniewski, J.; Ramshaw, H.; White, J.; Amad, M.; Korczak, B.; Petkovich, M. A novel human cytochrome P450, CYP26C1, involved in metabolism of 9-cis and all-trans isomers of retinoic acid. *J. Biol. Chem.* **2004**, *279*, 77–85.

(12) Ocaya, P.; Gidlof, A. C.; Olofsson, P. S.; Torma, H.; Sirsjo, A. CYP26 inhibitor R115866 increases retinoid signaling in intimal smooth muscle cells. *Arterioscler., Thromb., Vasc. Biol.* **2007**, *27*, 1542–1548.

(13) Loudig, O.; MacLean, G. A.; Dore, N. L.; Luu, L.; Petkovich, M. Transcriptional co-operativity between distant retinoic acid response elements in regulation of Cyp26A1 inducibility. *Biochem. J.* **2005**, *392*, 241–248.

(14) Vanwauwe, J. P.; Coene, M. C.; Goossens, J.; Vannijen, G.; Cools, W.; Lauwers, W. Ketoconazole Inhibits the Invitro and Invivo Metabolism of All-Trans-Retinoic Acid. *J. Pharmacol. Exp. Ther.* **1988**, *245*, 718–722.

(15) Acevedo, P.; Bertram, J. S. Liarozole Potentiates the Cancer Chemopreventive Activity of and the up-Regulation of Gap Junctional Communication and Connexin43 Expression by Retinoic Acid and Beta-Carotene in 10t1/2 Cells. *Carcinogenesis* **1995**, *16*, 2215–2222.

(16) Njar, V. C. O.; Gediya, L.; Purushottamachar, P.; Chopra, P.; Vasaitis, T. S.; Khandelwal, A.; Mehta, J.; Huynh, C.; Belosay, A.; Patel, J. Retinoic acid metabolism blocking agents (RAMBAs) for treatment of cancer and dermatological diseases. *Bioorg. Med. Chem.* **2006**, *14*, 4323–4340.

(17) Van Heusden, J.; Van Ginckel, R.; Bruwiere, H.; Moelans, P.; Janssen, B.; Floren, W.; van der Leede, B. J.; van Dun, J.; Sanz, G.; Venet, M.; Dillen, L.; Van Hove, C.; Willemsens, G.; Janicot, M.; Wouters, W. Inhibition of all-TRANS-retinoic acid metabolism by R116010 induces antitumour activity. *Br. J. Cancer* **2002**, *86*, 605–611.

(18) Stoppie, P.; Borgers, M.; Borghgraef, P.; Dillen, L.; Goossens, J.; Sanz, G.; Szel, H.; Van Hove, C.; Van Nyen, G.; Nobels, G.; Vanden Bossche, H.; Venet, M.; Willemsens, G.; Van Wauwe, J. R115866 inhibits all-trans-retinoic acid metabolism and exerts retinoidal effects in rodents. *J. Pharmacol. Exp. Ther.* **2000**, *293*, 304–312.

(19) Patel, J. B.; Huynh, C. K.; Handratta, V. D.; Gediya, L. K.; Brodie, A. M. H.; Goloubeva, O. G.; Clement, O. O.; Nanne, N. P.; Soprano, D. R.; Njar, V. C. O. Novel retinoic acid metabolism blocking agents endowed with multiple biological activities are efficient growth inhibitors of human breast and prostate cancer cells in vitro and a human breast tumor xenograft in nude mice. *J. Med. Chem.* **2004**, *47*, 6716–6729.

(20) Vasudevan, J.; Johnson, A. T.; Huang, D.; Chandrartna, R. A. U.S. Patent 6.252.090, 2005.

(21) Mulvihill, M. J.; Kan, J. L. C.; Cooke, A.; Bhagwat, S.; Beck, P.; Bittner, M.; Cesario, C.; Keane, D.; Lazarescu, V.; Nigro, A.; Nillson, C.; Panicker, B.; Smith, V.; Srebernak, M.; Sun, F. L.; O'Connor, M.; Russo, S.; Fischetti, G.; Vrkljan, M.; Winski, S.; Castelhano, A. L.; Ernerson, D.; Gibson, N. W. 3-[6-(2-dimethylamino-1-imidazol-1-yl-butyl)-naphthalen-2-yloxy]-2,2-dim ethyl-propionic acid as a highly potent and selective retinoic acid metabolic blocking agent. *Bioorg. Med. Chem. Lett.* **2006**, *16*, 2729–2733.

(22) Yee, S. W.; Jarno, L.; Gomaa, M. S.; Elford, C.; Ooi, L. L.; Coogan, M. P.; McClelland, R.; Nicholson, R. I.; Evans, B. A. J.; Brancale, A.; Simons, C. Novel tetralone-derived retinoic acid metabolism blocking agents: Synthesis and in vitro evaluation with liver microsomal and MCF-7 CYP26A1 cell assays. *J. Med. Chem.* **2005**, *48*, 7123–7131.

(23) Gomaa, M. S.; Yee, S. W.; Milbourne, C. E.; Barbera, M. C.; Simons, C.; Brancale, A. Homology model of human retinoic acid metabolising enzyme cytochrome P450 26A1 (CYP26A1): Active site architecture and ligand binding. *J. Enzyme Inhib. Med. Chem.* **2006**, *21*, 361–369.

(24) *Molecular Operating Environment*, version 2005.06; Chemical Computing Group: Montreal, QC, 2005.

(25) Molecular Operating Environment,version 2006.08; Chemical Computing Group: Montreal, QC, 2006.

(26) Ponder, J. W.; Case, D. A. Force fields for protein simulations. *Adv. Protein Chem.* **2003**, *66*, 27–85.

(27) Distance-dependent dielectric: $E_{SOL} = 0$, $E_{ELE} = q_i q_j / 4\pi\varepsilon_0 \varepsilon r_{ij}^2$

(28) Edelsbrunner, H. *Weighted Alpha Shapes*; technical paper of the Department of Computer Science; University of Illinois: Champaign, IL

(29) Aqvist, J.; Medina, C.; Samuelsson, J. E. New Method for Predicting Binding-Affinity in Computer-Aided Drug Design. *Protein Eng.* **1994**, *7*, 385–391.

(30) RAMPAGE server: http://mordred.bioc.cam.ac.uk/~rapper/rampage.php (accessed Dec 12, 2007).

CT800033X